Differential Photometry in Adaptive Optics Imaging

Szymon Gladysz
European Organisation for Astronomical Research in the Southern Hemisphere (ESO), Garching B. München, Germany

Roberto Baena Gallé
Department of Astronomy and Meteorology, University of Barcelona, Spain

Julian C. Christou
Gemini Observatory[1], Hilo Base Facility, Hilo, HI, USA

Lewis C. Roberts, Jr.
Jet Propulsion Laboratory[2], California Institute of Technology, Pasadena, CA, USA

ABSTRACT

One application of adaptive optics (AO) is high-resolution imaging of closely-spaced objects. Determining differential photometry between the two or more components of a system is essential for deducing their physical properties such as mass and/or internal structure. The task has implications for (i) Space Situational Awareness, such as the monitoring of fainter microsatellites or debris nearby a larger object, and (ii) astronomy such as the observations of close stellar faint companions. We have applied several algorithms to the task of determining the relative photometry of point sources with overlapping point spread functions in images collected with adaptive optics. These algorithms cover a wide range of approaches in the field of image processing. Specifically we have tested: PSF-fitting, multi-frame and single-frame blind deconvolution, maximum-likelihood approach combined with wavelet decomposition, and a novel one-dimensional deconvolution technique which separates signal and speckle statistics rather than integrated intensities. We present results from applying these algorithms to synthetic close binary stars for different observing conditions.

1. INTRODUCTION

Atmospheric turbulence imposes a limit on angular resolution which could be reached by ground-based telescopes. The application of astronomical adaptive optics (AO) during the last couple of decades has allowed diffraction-limited images, rather than seeing-limited, to be obtained with large ground-based telescopes. One of the uses of AO is high-resolution imaging of closely-spaced objects, e.g. binary stars or faint companions such as exoplanets. Determining the differential photometry and astrometry between the two components of the system is essential for deducing the physical properties of the components such as mass or internal structure [1]. AO, with a suitably bright guide star, improves the detectability and photometric accuracy but also introduces problems which are not usually encountered in conventional seeing-limited photometry [2]:

1. The structure of the PSF has temporal variation due to seeing variability. These morphological changes are difficult to model.
2. The AO long-exposure point spread function (PSF) in the medium- and high-correction regime shows long-lived quasi-static speckles. These diffraction-limited "lumps" are due to residual aberrations not sensed by AO (for example non-common-path errors) and lie in the halo surrounding the core of the PSF.

[1] The Gemini Observatory is operated by the Association of Universities for Research in Astronomy, Inc., under a cooperative agreement with the NSF on behalf of the Gemini partnership: the National Science Foundation (United States), the Science and Technology Facilities Council (United Kingdom), the National Research Council (Canada), CONICYT (Chile), the Australian Research Council (Australia), Ministério da Ciência e Tecnologia (Brazil), and Ministerio de Ciencia, Tecnología e Innovación Productiva (Argentina).

[2] The Jet Propulsion Laboratory is operated by the California Institute of Technology, under a contract with the National Aeronautics and Space Administration.

3. The AO corrected PSF, and the associated angular resolution on the sky, depend on the position of the science object relative to the AO guide star. AO compensates for the turbulence in the direction of the guide star and when the science object is well separated from the AO line of sight, the compensation suffers due to a different atmospheric volume. This effect is called angular anisoplanatism.

Because of these factors, extracting quantitative information from AO images is challenging. AO improves the detectability of faint companions over seeing-limited observations for a given telescope. When the companion is well separated with a non-overlapping PSF, aperture photometry takes care of all the problems mentioned above. The problems occur when the PSFs from each target overlap.

Esslinger and Edmunds [2] provide an excellent introduction to the problem of AO photometry. One of the issues discussed is the precision of photometry on deconvolved images compared with the PSF-fitting on the "raw" AO data. Two of the most-widely used deconvolution algorithms were tested, namely maximum entropy [3] and Richardson-Lucy [4,5]. For PSF-fitting the DAOPHOT package [6] was employed. Extensive testing on simulated faint companions showed that DAOPHOT performed consistently better than the deconvolution methods, i.e. its photometric precision was higher compared to precision of aperture photometry on the deconvolved images.

It has been suggested that AO observations should be processed with "myopic" deconvolution methods because the PSF is not well known for most AO observations [7]. For myopic deconvolution, it is assumed that the PSF is only partially known. In some cases the PSF is unknown and this is the regime for "blind" deconvolution. Typically these algorithms require an initial PSF estimate. This estimate is assumed to be close to the truth and the algorithm iterates this estimate until a common solution for both the object and the PSF is found. Myopic and blind deconvolution techniques often use regularization, e.g. by imposing object priors and PSF constraints [8]. Jefferies and Christou [9] developed an iterative blind deconvolution method guided by the minimization of a penalty functional. An important component for AO observations is the penalization of spatial-frequencies beyond the diffraction-limit of the observations. This package (IDAC) restores a "clean" image from which relative photometry and astrometry can be obtained by using aperture photometry with a very small aperture [2], or by model fitting. IDAC is one of the algorithms we have tested in our work.

PSF-fitting algorithms are applicable for crowded fields where the target comprises only point sources. In this approach an analytic or empirical PSF is used together with a fitting algorithm to match scaled-and-shifted copies of the PSF to the data. One such package suitable for AO imaging is StarFinder [10] which yields relative photometry and astrometry in AO-corrected crowded stellar fields. A PSF model is constructed from the brightest stellar images in the field. The algorithm iteratively uses this model to locate fainter sources which it then fits to extract the relative photometry and astrometry. There are three degrees of freedom: the total flux, and x and y positions for each component. The photometric and astrometric precision of StarFinder applied to crowded fields has been compared to results from blind deconvolution with the IDAC algorithm by Christou et al. [11]. We also test StarFinder's photometric accuracy in this paper.

A recent review of modern approaches to AO photometry [12] has demonstrated that methods utilizing static, deterministic PSF should not be dismissed against more modern algorithms like iterative blind deconvolution [13]. Thus in our set of methods to test we have included a new implementation of a Richardson-Lucy type deconvolution. This algorithm, Adaptive Wavelets Maximum Likelihood Estimator (AWMLE) [14], calculates an image that maximizes the compound Poisson and Gaussian likelihood of the data. It also performs wavelet decomposition that helps distinguish signal from noise which is important for improving the stopping rule. Unlike myopic or blind deconvolution AWMLE does not update the PSF so that it could be more dependent upon the initial PSF estimate.

A novel approach for measuring photometry of faint companions in AO imaging has been recently proposed [15,16]. In this method traditional 2-D image deconvolution is replaced by a 1-D time-series deconvolution. The algorithm is based on the observation that the statistical distribution of the peak of AO-corrected PSF is morphologically different from that of the off-axis light, i.e. the quasi-static speckles. This morphological difference between the two probability density functions (PDF) is used to constrain a one-dimensional, "blind," iterative deconvolution at the position of a faint companion to a star. Separation of the signal and speckle PDFs yields the differential photometry. The method ("PDF deconvolution"), has been successfully applied to medium-, and very-high-resolution AO observations [15,16]. We note that this PDF deconvolution has a rather narrow range of

applications as opposed to the other algorithms discussed here – it only produces photometry for AO observations of companions which lie within the uncorrected halo structure of the AO PSF. This algorithm requires the companion's location to be known. This can be obtained with a matching reference-less astrometric method [15] which then takes full-advantage of the self-calibrating nature of PDF deconvolution.

The goal of this paper is to focus on the description and usage of existing codes, and to compare their photometric precision after application to AO data in a "blind" test. We do not discuss all the issues pertaining to computing photometry in AO observations. Discussions which go into great depth on these subjects can be found in the literature [2,17].

2. METHODS

In this paper we compare results from the following algorithms, all of which were discussed above:

1. StarFinder: A PSF-fitting algorithm where the user-supplied PSF is iteratively fitted to the data assuming a double-delta object.
2. AWMLE: A Richardson-Lucy type approach with a static PSF.
3. IDAC: Multi-frame blind deconvolution.
4. FITSTARS: A single-frame iterative blind deconvolution.
5. PDF deconvolution: Using speckle statistics.

We have analyzed these algorithms for different AO correction scenarios. The AO correction is typically described by the Strehl ratio (SR). This is the peak of the AO-corrected PSF normalized to that of an ideal PSF for the same pupil. There are four scenarios: low vs. medium SR and "matched" vs. "mismatched" PSF. For the matched cases, the initial PSF has a similar SR to that of the observation and for the mismatched cases the initial PSF has SR with a difference of 6%. A detailed description of the data is given in Section 3.

2.1. StarFinder

StarFinder was developed to measure astrometry and photometry in crowded fields imaged with AO [10]. The algorithm operates as follows. Firstly, it derives a PSF template from the brightest isolated field stars and generates a catalogue of presumed objects by searching for the relative intensity maxima in the frame. Secondly, the images of the candidate stars are analyzed in order of decreasing peak intensity and each candidate is accepted on the basis of its correlation coefficient with the PSF template. The relative astrometry and photometry of each source are determined by means of a least-squares fit, taking into account the contribution of the local non-uniform background and of the already detected stars. These steps are repeated until no sources can be reliably found in the residuals. A thorough description of the algorithm, the IDL routines, GUI interface and excellent documentation can be found on the StarFinder's website[3]. For the results presented here, we used neither the graphical interface nor the capability of StarFinder to extract PSF from the data. Instead the algorithm was supplied with the observation, a "known" PSF (a single star observed after the target) and approximate positions of the two sources in the image via the FITSTARS.pro subroutine[4].

2.2. AWMLE

AWMLE [14,18] uses (i) Bayesian maximum-likelihood approach, (ii) wavelet transform (WT) [19], and (iii) multi-resolution support. The first maximizes the likelihood between the dataset and a possible solution by considering a combination of the intrinsic Poisson noise of the signal and the read-out Gaussian noise of the detector as well as describing the optical path by a static PSF that remains constant throughout the reconstruction process. The second decomposes the dataset into wavelet scales by means of the *à trous* algorithm [20]. The WT lets any signal or image be represented in N scales. This leads to simultaneous representation in both the measurement and frequency spaces. In general, the noise will mainly appear in the high spatial-frequency wavelet plane while broad shapes will appear in the low spatial-frequency planes. For AO observations, this permits differentiation between the diffraction-limited features (given by λ/D) and the seeing-limited scale (given *by* λ/r_0). An example of wavelet decomposition applied to

[3] http://www.bo.astro.it/~giangi/StarFinder/
[4] Not to be confused with the FITSTARS blind deconvolution code discussed later.

an AO PSF is shown in Figure 1. The third analyzes each wavelet scale in order to find significant WT coefficients that can be associated with real signal in an image. The standard deviation of intensity within a local window (whose size depends on the wavelet scale we are analyzing) is compared with the standard deviation of the whole plane. Their difference allows one to deduce the presence of a real source. This also helps to automatically stop reconstruction of the image at each wavelet scale independently.

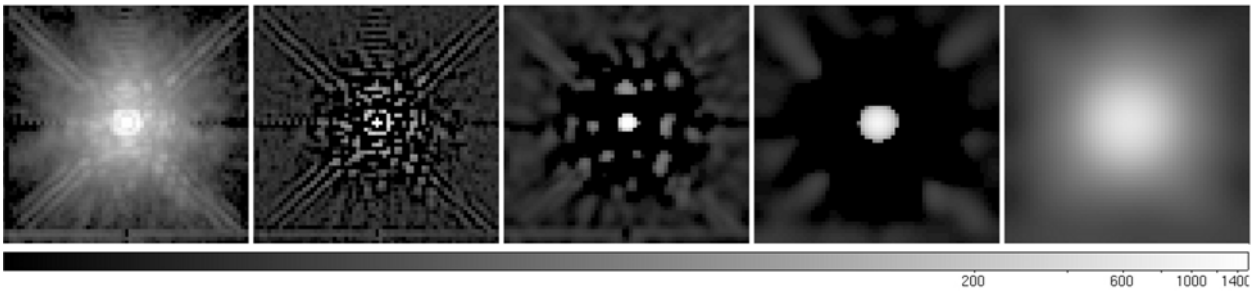

Fig. 1. Wavelet decomposition of the AO PSF. Left-to-right: AO PSF; three wavelet planes with decreasing spatial frequency and the lowest-frequency wavelet plane (the wavelet residual). (Displayed on a logarithmic scale.)

AWMLE was applied to the datasets using one wavelet scale plus a residual wavelet scale. A maximum number of 100 iterations were enough to achieve convergence in both scales. Note that AWMLE is not a photometric package. It produces a deconvolved image which can be subsequently analyzed by an observer. After reconstruction, aperture photometry, with a circle of five pixels in diameter, was used to extract the brightness of each component.

2.3. IDAC

IDAC is a multi-frame blind deconvolution (MFBD) algorithm[5]. Basically, it is an iterative least squares algorithm using a number of constraints to solve for both the common object (target) intensity distribution and also the corresponding PSFs for multiple observations of the same target [9,11]. MFBD algorithms are very successful in the case of strongly varying PSFs such as the pure speckle imaging case so that the target is easily distinguished from the PSFs. For AO data, the goal is to stabilize the PSF. This implies less PSF diversity from one observation to another so that other constraints become more useful.

In general, the algorithm makes no assumption of the target's intensity distribution and extent and the deconvolved image is computed for the full image plane. However, for the synthetic observations described in this paper, we have the prior knowledge that the target comprises two point sources and we also know their locations. What we do not know is the relative brightness between the two. In order to constrain the target to a binary star model, the initial target estimate comprises two narrow symmetric Gaussians centered on the pixel locations of the two targets, each having a FWHM = 1.75 pixels. This takes into account potential sub-pixel locations of the components and permits the algorithm to "shift" the component locations in order to obtain the best common fit. The initial intensity ratio of the two Gaussians is estimated from the corresponding pixel values in the observations and the initial PSF estimate was the "known" PSF described in Section 3. The PSF band-limit is typically measured from the data and read-noise limit was determined from "sky" regions of the observations. For this application ten independent observations were used for the multi-frame constraint. The algorithm was allowed to converge for ~100 iterations from the initial start-ups sharpening the Gaussian distributions of the two components and, more importantly, adjusting the relative amplitudes of both to allow the reconstructed target to match the ten individual data frames.

Like AWMLE, IDAC produces a final image from which photometric and astrometric measurements are made. For the binary cases here, the reconstructed object was fit by two Gaussians using a least squares method after a further Gaussian smoothing. This smoothing reduced the pixelation allowing for an improved fit. The free parameters for the fits were the amplitudes, elliptical Gaussian widths σ_x and σ_y, the position angle orientation of the ellipse and the x & y locations of each Gaussian - a total of 12 parameters in all. The intensity ratio was obtained from the ratio of the Gaussian volumes, (i.e. $V_n = I_n \sigma_x \sigma_y$). The advantage of the fitting is that it allows an uncertainty measurement for each of the intensity ratio.

[5] http://cfao.ucolick.org/software/idac/

2.4. FITSTARS

FITSTARS [13] is a single-frame iterative blind deconvolution algorithm optimized for binary stars by defining the object distribution as two δ-functions:

$$o(x,y) = \sum_{i=1}^{2} A_i \delta(x - x_i, y - y_i). \quad (1)$$

where (x_i, y_i) is the location of the i_{th} component and A_i its intensity so that there are a total of six object variables to fit. These binary parameters are solved for by using least squares fitting to the observations using the initial target and PSF estimates. Once an initial estimate of these variables is obtained, an updated PSF estimate for each component is computed by differencing the measurement to the model for the other component and a new PSF estimate is then computed from the weighted average of these two individual component estimates [21]. This process is repeated until the results converge. Results using this algorithm have been compared to those obtained by speckle interferometry [22] and are in good agreement.

2.5. PDF deconvolution

PDF deconvolution uses the analytical forms of the PDFs of the on-axis and off-axis intensity in an AO PSF [16]. The instantaneous Strehl ratio has a distribution characterized by two parameters (i) number of independent cells in the AO-corrected wavefront, and (ii) the theoretical long-exposure Strehl ratio, which is related to the statistical phase variance via the extended Maréchal approximation $\mathrm{SR} = \exp\left(-\sigma_\phi^2\right)$ [23]. When the companion is located within the isoplanatic patch, both components of a binary star are produced by almost the same wavefront. Thus, the two parameters mentioned above are common for the PDFs of the peak intensity of the star and its companion. However, at the location of the companion, the speckle and signal intensities add, and their PDFs are convolved. The distribution of the signal (i.e. the "raw" peak intensity) has the same form as the Strehl ratio PDF [16] but is "blurred" by the speckle kernel. PDF deconvolution blindly estimates both the signal and the speckle PDFs from a vector of intensity measurements at the location of the companion.

This 1-D deconvolution problem has five parameters to solve for but can be very easily constrained by observing that two parameters are common for both objects, i.e. those of the instantaneous SR. These are obtained from a least-squares fit of the theoretical PDF to the on-axis statistics for the bright star so that, at the location of the companion, the algorithm only searches for the three remaining parameters. After successful separation of signal from speckle statistics differential photometry can be obtained by comparing flux parameters estimated for the two objects.

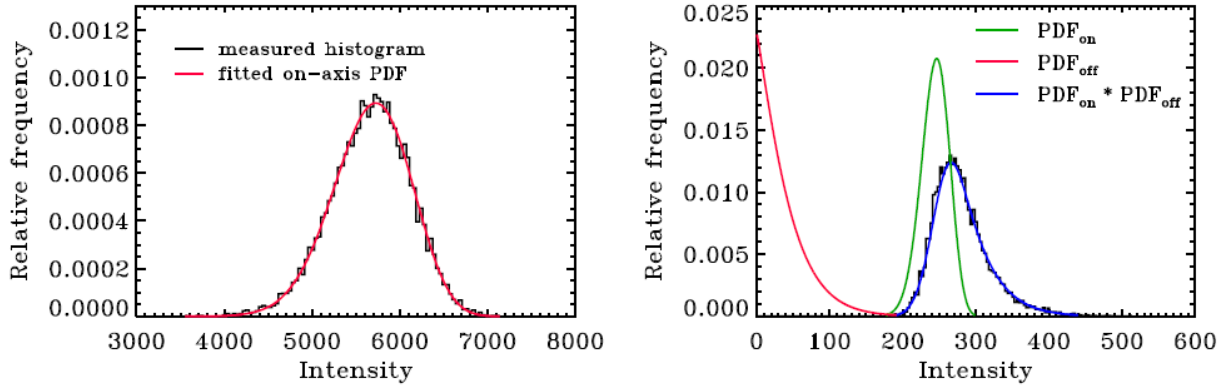

Fig. 2. PDF deconvolution. Left: fit of the theoretical on-axis PDF to the measured histogram. Right: separation of the PDFs at location of a companion. PDF_{on} is the on-axis distribution; PDF_{off} is the speckle distribution. Symbol "*" denotes convolution. This plot corresponds to a typical case encountered in tests on the Lick data, as described in Section 3.

PDF deconvolution relies on multi-frame observations of the object. The other inputs are the estimated Strehl ratio of the observations, and the position of the companion (assumed to be known from astrometry). Figure 2 illustrates

how the method works. First, the theoretical on-axis PDF is fit to the measured on-axis histogram (left panel), and then the convolution of two PDFs is fit to the measured histogram at the location of the companion (right panel). The ratio of the widths of the two distributions of interest (red curve in the first panel and green curve in the second panel) can be converted to brightness ratio of the two objects.

In this work the PDF deconvolution algorithm is supplied with the known positions of the companions which it does not update. When the peak of the companion's PSF is at a sub-pixel location, the method is given a non-integer location of the companion and it spatially interpolates the measured pixel values to extract the intensity time series for the PDF.

3. DESCRIPTION OF THE DATA

We used single-star data sets, obtained with the Lick Observatory AO system on the 3m Shane telescope to generate synthetic binary stars. AO images of bright stars were obtained using the high-speed sub-array mode (64 × 64 pixels), for the 256 × 256 pixels IRCAL camera, which corresponds to a field size of 4.8 × 4.8 arcsec. The sub-array measurements were captured with typical exposure time of 22ms. Each data set comprised 10,000 images. All data were obtained in K band (2.2μm) where the diffraction limit is 151mas and the data were effectively Nyquist sampled (two pixels per λ/D). The individual short exposures were registered with sub-pixel accuracy to produce shift-and-add (SAA) images. The average Strehl ratio of these SAA images was ~ 40%. All data were sky-subtracted and the residual background was then subtracted too.

Fig. 3. SAA image of a synthetic binary star with separation of 4λ/D. Left: High SR (~50%) showing the eight locations for the artificial companion. The companion is located within the larger circle. Right: SAA image of the synthetic binary star for SR ~ 30%. Note the presence of significantly greater residual speckle structure for SR~50% whereas the SR~30% shows a more uniform halo structure. (The images are displayed on logarithmic scale).

Simulated binary star data sets were created by scaling and shifting the PSF datacubes yielding synthetic observations of a binary star with a brightness ratio of 25 (magnitude difference, Δm = 3.5) which was chosen to create challenging scenarios, with 5 < SNR < 15 for the companion. We placed the companion at one of eight different positions in order to minimize variations in results due to possible anisotropies in the PSF. The positions were ~ 0.6 arcsec (4λ/D) from the center of an image (see Figure 3) with four positions in a cross 8 pixels away horizontally or vertically from the bright star, and four diagonally – 7 pixels horizontally and 4 pixels vertically. The difference between the "straight" and "diagonal" separations is 0.062 pixel. The mean photometric error was computed based on the results from these eight positions.

All algorithms were supplied with re-centered images. PDF deconvolution used a 10,000 frame datacube, IDAC used 10 data cubes, each comprising 1000 co-added frames, while the other codes used single SAA images of all 10,000 frames. All methods, except PDF deconvolution, rely on a PSF estimate. For the matched-PSF cases we used the same stars observed ten minutes later (Strehl ratio mismatch = 2 or 3%). For the mismatched-PSF cases we used stars of similar brightness observed the same night, and also close to zenith (Strehl ratio mismatch = 6%; for the case of ~30% SR the calibrator had higher SR than the target while the reverse situation was tested for 50% SR). Variability of the Strehl ratio between the science and calibration PSF is a direct consequence of either non-

stationarity of turbulence (if the same star was used for target and calibration datasets), or change in response of the AO system due to lower or higher photon flux coming from the calibrator, as compared to the target. Table 1 summarizes the grid of scenarios we have investigated.

Table 1. PSFs used to simulate images of binary stars. The SR = 29% data refers to the 30% Strehl ratio case, and the SR = 54% data to the Strehl ratio = 50% case in the text.

	Science PSF	Strehl ratio	m_V	m_K	Reference PSF	Strehl ratio	m_V	m_K
Matched PSF	NOMAD1 1297-0510182	29%	12.1	5.93	—	32%	—	—
Mismatched PSF	—	—	—	—	HD 18009	35%	8.23	5.02
Matched PSF	HD 143209	54%	6.3	3.92	—	52%	—	—
Mismatched PSF	—	—	—	—	HD 153832	48%	7.25	4.78

4. RESULTS

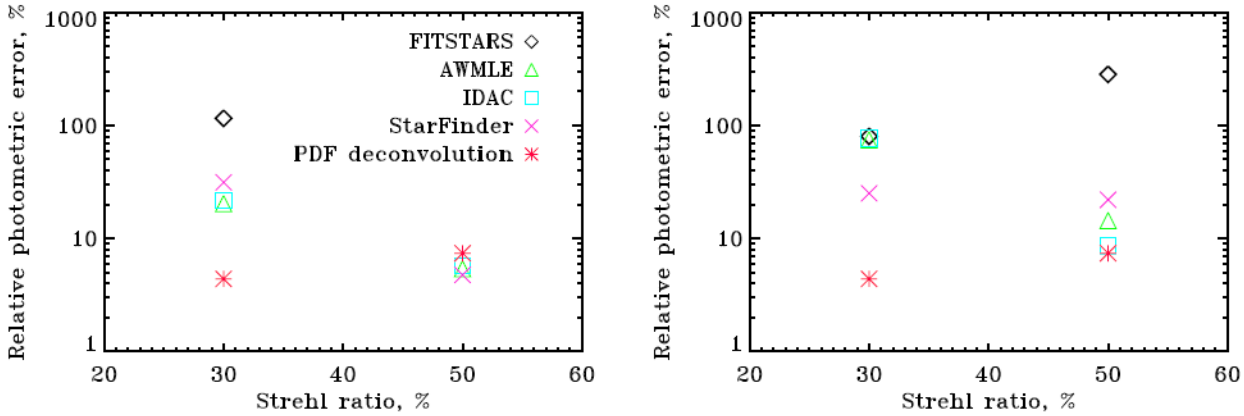

Fig. 4. Mean relative intensity ratio error for the five algorithms (equation 3). Left: PSF well-matched to the observations. Right: mismatched PSF. The results for PDF deconvolution are identical in both panels because this method does not rely on a PSF estimate. The p_2 value for FITSTARS in the 50% SR, matched-PSF case was very high (~ 10 000) and we omitted it from the plot in order to have the y-axis scale which better shows differences between the other methods.

In order to determine the efficacy of each algorithm we used a metric of photometric precision which measured the mean absolute deviation from the truth [12]:

$$p_1 = \frac{1}{8}\sum_{j=1}^{8}\left|I_j - \text{truth}\right| \tag{2}$$

where I_j are the individual intensity ratio measurements and the **truth** was equal to 25. This metric was then converted to percent relative error:

$$p_2 = \frac{p_1}{\text{truth}} \times 100\% \tag{3}$$

This metric shows the relative strength of the average departure from the true intensity ratio. In Figure 4 we plot p_2 for the scenarios of well matched and mismatched PSF and in Table 2 we give numerical values of this metric.

Figure 4 illustrates relative *precision* of various algorithms. In order to discuss possible *biases* (systematic over-, or under-estimation of the truth) and *dispersions* of results, we plot means and standard deviations in Figure 5 and we give numerical values of these metrics in Table 3.

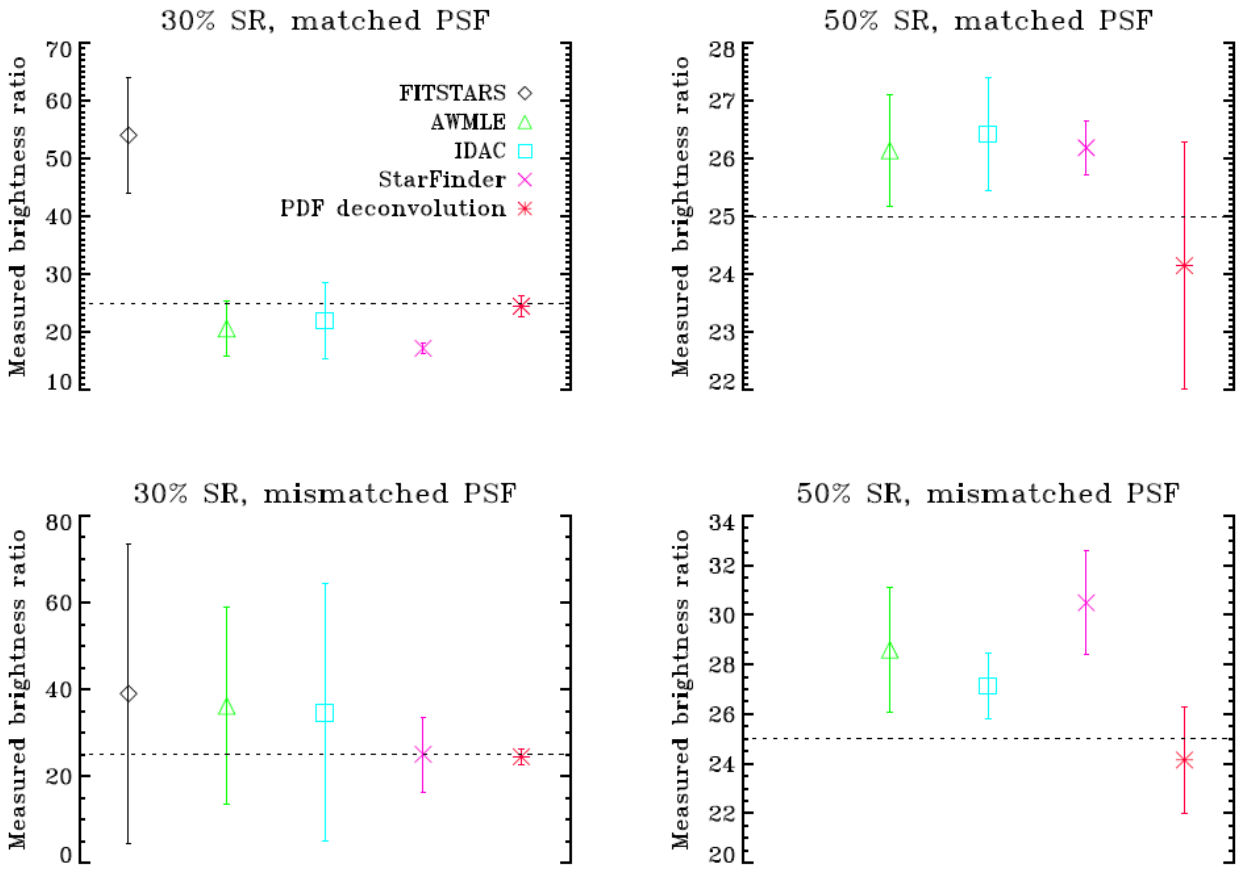

Fig. 5. Means and standard deviations of the measured brightness ratios. The dashed line corresponds to the true value of 25. The values for FITSTARS in the matched-, and mismatched-PSF cases for 50% SR were very high and we omitted them from the plots in order to emphasize differences between the other methods. The PDF deconvolution, being self-calibrating was independent of the PSF and therefore it produced the same results for the matched and mismatched PSFs. (Note the differences in the vertical scales).

Table 2. Percentage photometric precision of the algorithms, as quantified by the metric p_2.

	FITSTARS	AWMLE	IDAC	StarFinder	PDF deconvolution
30% SR, matched PSF	116	20	21	31	4
50% SR, matched PSF	10848	5	6	5	7
30% SR, mismatched PSF	80	75	77	25	4
50% SR, mismatched PSF	284	14	8	22	7

Table 3. Means and standard deviations of brightness ratios obtained with the discussed methods.

	FITSTARS	AWMLE	IDAC	StarFinder	PDF deconvolution
30% SR, matched PSF	54.0 ± 10.0	20.6 ± 4.7	21.9 ± 6.5	17.1 ± 0.9	24.4 ± 1.8
50% SR, matched PSF	2737 ± 4275	26.1 ± 1.0	26.4 ± 1.0	26.2 ± 0.5	24.1 ± 2.1
30% SR, mismatched PSF	38.9 ± 34.5	36.1 ± 22.6	34.6 ± 29.6	25.0 ± 8.6	24.4 ± 1.8
50% SR, mismatched PSF	96.0 ± 124.2	28.6 ± 2.5	27.1 ± 1.3	30.5 ± 2.1	24.1 ± 2.1

5. SUMMARY & DISCUSSION

We compared photometric measurements of various algorithms for a case of a very close binary star with a relatively large intensity ratio. This is a particularly challenging case in that the companion is 25x fainter than the primary and lies well within the PSF morphology of the primary (~4 λ/D). This is where the speckle contribution is non-negligible and the best photometric precision (Fig. 4) is on the order of couple of percent relative to the truth. For each observing case there were eight different realizations with the companion located in a different region of the primary's PSF and the dispersion in the results reflect the sensitivity of the algorithms to measure the photometry with differing speckle backgrounds and morphology.

Looking at the results in Fig. 5 and Table 3, one notices that for the SR=50% case, the mean IDAC, StarFinder and AWMLE results are very similar to each other and consistently give a larger intensity ratio by ~ 4% for the matched PSF and by ~ 7% for the mismatched PSF. Note the overlap of the standard deviations. For the PDF deconvolution, which is independent of any separate PSF information, the results are < 4% smaller than the true intensity ratio. However, for FITSTARS, the results are ~ 100x and 4x larger. For these data, FITSTARS had problems. For the SR=30% data, IDAC, StarFinder and AWMLE underestimate the intensity ratio ~ 20% for the matched PSF, and IDAC and AWMLE overestimate by ~ 40%, whereas StarFinder yields the correct value, for the mismatched PSFs. PDF deconvolution underestimates the truth by ~ 4% in both cases. It is interesting to note that FITSTARS yields significantly improved results for these data overestimating by ~ 1.5x. Finally we note that the dispersions increase in the majority of mismatched PSF cases.

So, why do these algorithms differ so much in their results? Non-linear deconvolution algorithms, such as AWMLE and IDAC, have a tendency to overestimate intensity ratios when the intensity ratio is large to begin with. This has been shown by Christou et al. [11] and in presentations by various authors in the proceedings of the HST workshop [24]. This is essentially due to the reduced SNR of the fainter sources. Also some of the algorithms compute the astrometry of the target jointly with the photometry and when the astrometric errors are large, so are the photometric errors. For example, StarFinder converged for only four of the eight realizations for the SR=30% mismatched PSF case and FITSTARS converged for six of the eight realizations for the SR=30%, matched PSF case. PDF deconvolution is not influenced by astrometric errors as the true binary component locations are used. In addition, not all algorithms are well matched to these data. For example FITSTARS assumes that the reconstructed PSF is symmetric after a certain radius which could well affect the results here, because of the binary star separation relative to the size of the extended PSF. The different algorithms also use the data in different ways. FITSTARS, StarFinder and AWMLE used a single SAA image obtained from the original 10^4 data frames while IDAC used ten 10^3 SAA images to take advantage of the MFBD approach and PDF deconvolution used the 10^4 frames for the statistical distributions. We have not yet investigated the repeatability of these algorithms by breaking the data into smaller subsets to investigate how that affects the mean results.

Another difference to note is that the binary parameters themselves are estimated differently for each of the PSF calibration algorithms. Aperture photometry, centered on the component locations, is used for the AWMLE result. For the SR=30% case there is greater speckle contamination of the companion thus affecting the results. The presence of a deterministic mask using the component locations should improve the results by rejecting the speckles. StarFinder jointly estimates the relative astrometry and photometry parametrically and it was found that if the initial estimate of the companion's location was more than 0.5 pixels away from its true location, then the algorithm would not converge. FITSTARS also jointly estimates the binary parameters directly and is sensitive to the astrometric positions. IDAC estimates an object intensity distribution and the use of an initial Gaussian model centered on the component locations ensured that this was limited to the correct locations. The binary parameters were obtained by fitting the final Gaussian result where the formal error of the least squares fit for the intensity ratio was ~ 2%, substantially smaller than the results for the eight different realizations. For the SR=30% mismatched PSF case, the asymmetric nature of the PSF led to increased speckle contamination in the results for a couple of the realizations so that the mean was skewed and the standard deviation was increased.

By comparison to the PSF calibration algorithms, PDF deconvolution is self-calibrating and relies on how well the speckle statistics are determined in order to estimate the relative intensities. The ability to determine the statistics of the intensity is directly related to the number of samples, i.e. the number of frames. How well such an algorithm will

work with a small number of frames is yet to be determined as is the maximum exposure time per frame before the central-limit theorem dominates producing indistinguishable Gaussian statistics.

We have presented preliminary results of the algorithms' application to these challenging data. Future studies will investigate the sensitivity of the PSF calibration methods to different initial PSF estimates, the repeatability of all techniques and the sensitivity of the multi-frame algorithms, IDAC and PDF deconvolution, to the number of frames.

Acknowledgements

This work is sponsored by the Air Force Office of Scientific Research, Air Force Materiel Command, USAF, under grant no. FA8655-09-1-3052, and the Spanish Ministry of Science and Technology under grants no. AyA-2005-08604 and AyA-2008-01225. Roberto Baena has a research fellowship (FPI) from the MCyT no. BES-2006-11903.

The U.S. Government is authorized to reproduce and distribute reprints for Governmental purpose notwithstanding any copyright notation thereon.

6. REFERENCES

1. Vigan A., Moutou C., Langlois M., Allard F., Boccaletti A., Carbillet M., Mouillet D., Smith I., "Photometric characterization of exoplanets using angular and spectral differential imaging", Monthly Notices of the Royal Astronomical Society, 407, 71–82, 2010.
2. Esslinger O., Edmunds M. G., "Photometry with adaptive optics: A first guide to expected performance", Astronomy & Astrophysics Supplement Series, 129, 617-635, 1998.
3. Frieden B. R., "Restoring with maximum likelihood and maximum entropy", Journal of the Optical Society of America, 62, 511-518, 1972.
4. Richardson W. H., "Bayesian-based iterative method of image restoration", Journal of the Optical Society of America, 62, 55-59, 1972.
5. Lucy, L. B., "An iterative technique for the rectification of observed distributions", Astronomical Journal, 79, 745-754, 1974.
6. Stetson, P. B., "DAOPHOT - A computer program for crowded-field stellar photometry", Publications of the Astronomical Society of the Pacific, 99, 191-222, 1987.
7. Pantin E., Starck J. L., Murtagh F., "Deconvolution and blind deconvolution in astronomy" in *Blind image deconvolution: theory and applications*. Egiazarian K. and Campisi P. (Eds), CRC Press, 277-317, 2007.
8. Mugnier L. M., Fusco T., Conan J.-M., "MISTRAL: a myopic edge-preserving image restoration method, with application to astronomical adaptive-optics-corrected long-exposure images", Journal of the Optical Society of America A, 21, 1841-1854, 2004.
9. Jefferies S., Christou J. C., "Restoration of astronomical images by iterative blind deconvolution", Astrophysical Journal, 415, 862-874, 1993.
10. Diolaiti E., Bendinelli O., Bonaccini D., Close L., Currie D., Parmeggiani G., "Analysis of isoplanatic high resolution stellar fields by the StarFinder code", Astronomy & Astrophysics Supplement Series, 147, 335-346, 2000.
11. Christou, J. C., Pugliese, G., Köhler, R., Drummond, J. D., "Photometric and astrometric analysis of Gemini/Hokupa'a galactic center adaptive optics observations", Publications of the Astronomical Society of the Pacific, 116, 734-744, 2004.
12. Burke D., Gladysz S., Roberts L., Devaney N., Dainty C., "An improved technique for the photometry and astrometry of faint companions", Publications of the Astronomical Society of the Pacific, 121, 767-777, 2009.
13. ten Brummelaar, T. A., Mason, B. D., McAlister, H. A., Roberts, L. C., Jr., Turner, N. H., Hartkopf, W. I., Bagnuolo, W. G., Jr., "Binary star differential photometry using the adaptive optics system at Mount Wilson Observatory", Astronomical Journal, 119, 2403-2414, 2000.
14. Otazu, X., PhD thesis, University of Barcelona, 2001.
15. Gladysz S., Christou J. C., "Reference-less detection, astrometry, and photometry of faint companions with adaptive optics", 2009, Astrophysical Journal, 698, 28-42, 2009.
16. Gladysz S., Yaitskova, N., Christou J. C., "Statistics of intensity in adaptive-optics images and their usefulness for detection and photometry of exoplanets", Journal of the Optical Society of America A, 27, A64-A75, 2010.
17. Roberts, L. C., Jr., Turner, N. H., Bradford, L. W., ten Brummelaar, T. A., Oppenheimer, B. R., Kuhn, J. R., Whitman, K., Perrin, M. D., Graham, J. R. "Adaptive optics photometry and astrometry of binary stars", Astronomical Journal, 130, 2262-2271, 2005.
18. Fors, O., PhD thesis, University of Barcelona, 2006. http://www.tdx.cesca.es/TDX-0330106-125745/
19. Daubechis, I., "Ten lectures on Wavelets" (Philadelphia), 1992.
20. Shensa, M. J., "The discrete wavelet transform: wedding the á trous and Mallat algorithms", IEEE Trans. Signal Processing, 40, 2464-2482, 1992.
21. ten Brummelaar T. A., Mason, B. D., Bagnuolo, W. G., Jr., Hartkopf, W. I., McAlister, H. A., Turner, N. H., "Differential binary star photometry using the adaptive optics system at Starfire Optical Range", Astronomical Journal, 112, 1180-1187, 1996.
22. Horch, E., Ninkov, A. Z., Franz, O. G., "CCD speckle observations of binary stars from the southern hemisphere. III. Differential photometry", Astronomical Journal, 121, 1583-1596, 2001.
23. Hardy, J. W., "Adaptive optics for astronomical telescopes" (Oxford University Press, Oxford, UK), 1998.
24. The Restoration of HST Images & Spectra II, R.J. Hanisch & R.L. White, Ed., 212-218, 1994.